The Nuclear Schiff Moment in ^{205}TlF: Microwave Generation and Implementation

Jonah Majumder

under the supervision of Professor Dave DeMille

May 4, 2017

Abstract

This project concerns the generation and implementation of microwaves for Professor Dave DeMille's experiment to measure the nuclear Schiff moment in ^{205}TlF. Microwaves signals, used to transfer molecules between energy states, are integral to the preparation and measurement stages of the experiment. Effective use of microwaves in this experiment requires both precisely controllable generation and implementation of the signals. To address the generation aspect, microwave signals are digitally synthesized to modulate frequency and couple hyperfine levels. To implement these microwaves, a quasi-optical cavity is used. Using partially-transmitting mirrors for coupling, this cavity will allow us to circulate large amounts of microwave power uniformly. The design and evaluation of this cavity have been the major focus of my work this semester.

Contents

1 Introduction

This experiment, designed to search for a nuclear Schiff moment in Thallium Fluoride, is one of a few experiments in which Professor DeMille's group is involved. It is on the cutting edge of atomic physics and will potentially grant new insights into unexplained physical phenomena in our universe. This experiment, however, is still in its beginning stages. Many of the necessary components have not yet been assembled, and the experiment is not expected to yield valuable data for a few years. My work has been focused on designing and helping to implement a few necessary components of the experiment, namely those involving microwave signals. The theory and designs detailed in this report are based on conversations with Professor DeMille and other helpful members of his group, as well as proposals and posters made for the experiment.

2 Background

2.1 The Schiff Moment

The Schiff moment is an electric dipole moment arising from a charge asymmetry along the spin axis of the proton. Such an asymmetry implies that when we apply the time-reversal operator ($\hat{\mathrm{T}}$: $t \mapsto -t$), the Hamiltonian of the system is fundamentally altered. For this reason, we say that this charge asymmetry *violates time-reversal symmetry*. The Standard Model of particle physics predicts a small amount of time-reversal symmetry violation, but the relative amounts of matter and antimatter detected in the universe suggest that there may be more such violation present in nature. The electric dipole moment we seek to measure in this experiment could provide evidence for this suspicion and suggest an improvement to the Standard Model.

2.2 Using ^{205}TlF

The Thallium Fluoride molecule used in this experiment has a number of desirable characteristics. This experiment seeks to detect and measure the Schiff moment in the nucleus of the ^{205}Tl atom. TlF is a very polar diatomic molecule, with a large internal electric field. This means that the molecule will be highly polarizable by a laboratory electric field. In addition, the molecular energy level structure of TlF is well suited for the optical cycling and state transfer necessary in multiple stages of the experiment. The presence of a nearly-closed optical cycling transition in TlF ensures that the fraction of molecules that are not properly prepared, focused, and detected will be small. Next, the sensitivity to the Schiff moment scales as $A^{2/3}Z^2$, where A is the nuclear mass number and Z, the nuclear charge. ^{205}TlF takes advantage of this relation, with relatively large values for both of these factors. Lastly, the structure of the Thallium nucleus is such that there is a single unpaired valence proton. This means that the experiment will yield an upper limit on the electric dipole moment of the proton, among other parameters.

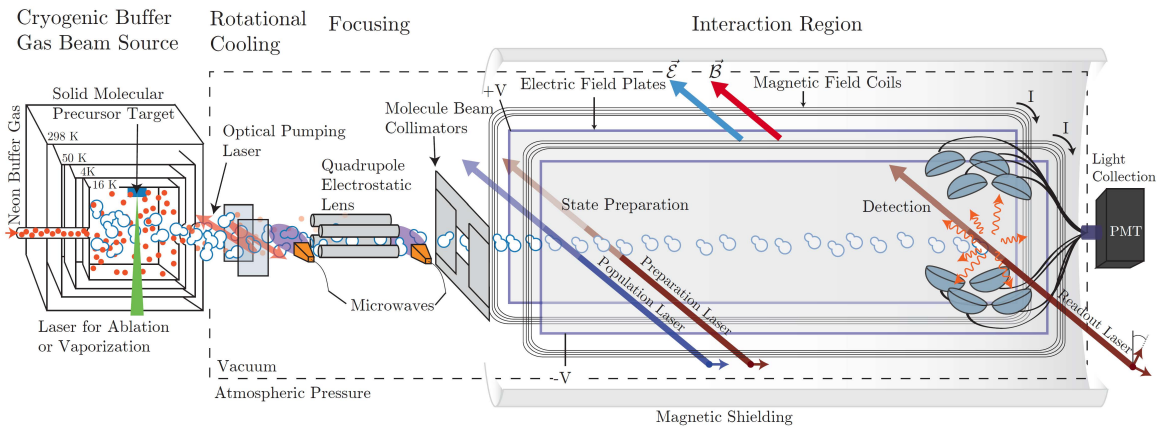

Figure 1: Experimental layout.

2.3 Discussion of Previous Results

There have been a few experiments seeking to measure similar subatomic effects in the past. In 1991, D. Cho, K. Sangster, and E. A. Hinds performed measurements in a very similar experiment [1], also seeking to measure the Schiff moment in TlF. However, our experiment differs in its use of a cryogenic buffer gas beam source and the optical cycling stage mentioned above. These changes are expected to significantly improve the detection rate and sensitivity of the experiment. Multiple experiments have also been carried out measuring the Schiff moment in the nucleus of ^{199}Hg [2] [3], but such measurements are limited by the smaller polarizability of a single atom. Diatomic molecules, in contrast, carry internal electric fields and therefore have higher intrinsic sensitivity to electric forces.

For reference, the sensitivities of EDM and Schiff moment measurements scale as:

$$\mathcal{P}\,\tau\,\sqrt{\dot{N}}\,\mathcal{S}$$

Overall sensitivity with respect to various previous experiments is improved through each of these elements independently. $\mathcal{P}$, the electric polarization, is improved through the polarizability of diatomic atoms; τ, the interaction time, is increased with a longer interaction region and better slowing methods; the detection rate $\dot{N}$ is improved by optical cycling; and $\mathcal{S}$, the intrinsic sensitivity of the system to the Schiff moment, improves with larger Z and A, as mentioned above.

3 Experimental Overview

A diagram of the experimental setup is shown in Figure 1. Generally speaking, the experiment can be divided into the stages of molecular beam production, molecular preparation and focusing, spin precession (i.e. the interaction), and detection.

3.1 Beam Production

TlF molecules are produced by ablating a solid TlF target with a laser. The resulting flux of molecules is cooled by a buffer gas of Helium, and the TlF molecules emerge from the source at a temperature of 4 K. Similar methods of producing molecular beams have been successfully demonstrated in the past [4]. Upon emerging from the beam source, the TlF molecules populate multiple different states. According to the Boltzmann distribution of energies, these molecules essentially just occupy energy states associated with quantum number $J = 0, 1, 2, 3$. (J is the quantum number associated with the orbital angular momentum of the F nucleus about the Tl nucleus.) Furthermore, the molecules may occupy a number of different hyperfine sublevels (denoted by quantum number F).

3.2 Laser Cooling

Later stages require molecules in the state with $J = 0$, $F = 0$, which we achieve through a process known as rotational "cooling." Rotational cooling is a process which methodically empties out undesired states of molecules. Using a UV laser, we excite molecules out of the $J = 2$ state into an (electronically) excited state with $J' = 1$. After being excited, these molecules decay back down into one of our original J states. We can be sure that this decay (i.e. spontaneous emission) will occur relatively quickly because the energy differences between J and J' states are very large compared to those within electronic states. If the state into which a molecule decays happens to be the $J = 0$, $F = 0$ state, it is left alone; otherwise, microwaves drive transitions to ensure that the molecule returns to the $J = 2$ state, so it can be re-excited. The result of this process, when continually allowed to run, is the accumulation of molecules in our desired state.

3.3 Beam Focusing

Focusing of the molecular beam is crucial because over a long spatial distance, poorly focused beams can diverge considerably and reduce detection. We use what is called an "electric quadrupole lens" to accomplish focusing, which is essentially four charged rods in a square formation, with charge alternating (+), (−), (+), (−). The resulting electric field leverages the Stark effect to impose a potential that confines the molecules spatially to the center. It turns out that the focusing effect here is strongest with moelcules in the state $J = 3$, $m_J = 1$. However, once rotational cooling has brought all molecules to the $J = 0$, $F = 0$ state, it becomes straightforward to transfer molecules between states using microwave signals. A DC electric field is applied here to resolve different m_J sublevels.

3.4 Molecule Preparation

Following the focusing portion of the experiment, the interaction region of our experiment requires molecules in the $J = 1$, $m_J = \pm 1$. This requires yet another stage of rotational state transfer. Finally, another electric field is applied in order to orient the molecules. When the

TlF molecules finally enter the interaction region, an electric field polarizes the molecules, granting external control over the orientation of the huge internal electric field. Recall that the spin of the entire Tl nucleus is equivalent to the spin of a single valence proton in that nucleus, so can be described in a classic spin-$\frac{1}{2}$ framework.

3.5 Spin Precession

When the TlF molecules enter the interaction region, they all have their Tl nuclei in the $|+z\rangle$ spin state, where $+z$ is defined to be along the internal electric field of the molecule. Immediately after entering the interaction region, the molecules pass through a coil of radiofrequency oscillating current. The oscillating magnetic field performs a $\frac{\pi}{2}$-rotation about the $+y$ axis on the Tl nuclear spin state. This rotates the spin vector from $|+z\rangle$ to $|+x\rangle$, essentially taking advantage of the property of nuclear magnetic resonance.

Over time, the Tl nuclear spin vector evolves as dictated by the time-dependent Schrodinger equation. Without the effects caused by the Schiff moment, this vector would stay still over time. However, the Schiff (dipole) moment causes the spin vector of the Tl nucleus to interact with the internal electric field of the molecule, inducing an energy difference between the $|+z\rangle$ and $|-z\rangle$ eigenstates. This splitting causes the Tl spin vector to rotate around the x-y plane, in a phenomenon called "spin precession." This precession causes what was initially a pure $|+x\rangle$ state to become a mixture of $|\pm x\rangle$ and $|\pm y\rangle$ states.

Before the molecules exit the interaction region, they pass through a second set of radiofrequency coils, whose oscillating magnetic field again rotates the Tl nuclear spin state again. This time it is rotated by $\frac{\pi}{2}$ about the $-x$ axis, projecting the final y component of the spin vector onto the z axis.

3.6 Detection

In the detection stage, our task is simply to estimate the expectation value of the z component of the final Tl nuclear spin. We know that this expectation value (after the $\frac{\pi}{2}$-rotation) must have been exactly the expectation value of the y component before the rotation. Furthermore, we know that the expectation value of spin in the y direction oscillates throughout the interaction region with the precession of the spin vector.

Unfortunately, the projection of the Tl nuclear spin vector onto the z axis is not a directly measurable value. In measuring the Tl nuclear spin, we collapse its wavefunction and force the spin to "choose" either $|+z\rangle$ or $|-z\rangle$. However, as the number of spin measurements increases, we also know that our estimate, based on the fraction we find in the $|+z\rangle$ state, will approach the true value of $\langle \hat{S}_z \rangle$.

Measurement of the Tl nuclear spin for each molecule is accomplished through a sequence of clever steps. Microwave signals couple only the $|-z\rangle$ state with rotational state $J = 2$ (recall that up to this point, all molecules have $J = 1$). After this state transfer, the states of $|+z\rangle$ and $|-z\rangle$ are essentially mapped onto $J = 1$ and $J = 2$. Next, "state readout" lasers successively excite molecules from the $J = 1$ state and the $J = 2$ state, and photomultiplier tubes are used to collect and record the emission of photos as the excited states decay.

Counting these photons reveals the fraction of molecules in the $J = 1$ and $J = 2$, and therefore the $|+z\rangle$ and $|-z\rangle$ states. From here, it is straightforward to infer how much the Tl spin vector precessed and calculate the magnitude of the Schiff moment.

4 Usage of Microwave Signals

As the previous sections of this report indicate, practically every stage of this experiment requires microwave signals for rotational state transfer. We require microwaves in of a variety of frequency regimes, from the gigahertz range for rotational state energy differences, to megahertz- and even kilohertz-range signals for splitting in the hyperfine sublevels. One of the greatest experimental challenges we face is to cost-effectively and practically *generate* and *implement* microwave signals. My work over the last year has primarily been focused on these two goals.

4.1 Microwave Generation

The number of molecular transitions that we'd like to address far exceeds the number of independent signals that we can reasonable produce. Our solution to this problem is to modulate signals (in frequency) over time, *successively* coupling necessary levels. If we are able to switch between frequencies precisely enough, and at a fast enough rate, we can achieve the same effect as if we had many independent signals. Over the last semester (and the previous summer) I worked to build an apparatus to produce and control such microwave signals, using a method called direct digital synthesis.

Direct digital synthesis (DDS) is a technique to generate an arbitrary analog signal from a fixed frequency reference source. I built a software and hardware interface to use DDS to meet our signal generation needs. The hardware interface made use of an evaluation board made by Analog Devices, with a metal casing to protect and facilitate use of the device in the lab. Then, I wrote a series of LabVIEW programs to control the device in a simple and intuitive fashion. Although the signals produced by this apparatus are limited to the megahertz regime, we can achieve frequency modulation in the gigahertz range simply by mixing the output with a higher-frequency carrier signal.

4.2 Microwave Implementation

To expose the molecular beam to these microwaves, we use quasi-optical cavities. The majority of my work this semester has been aimed at characterizing such a cavity in order to fully understand its operation. The use of a microwave cavity allows us to confine microwave signals spatially, ensuring that stray signals do not cause unintended effects elsewhere. In addition, the fact that we can resonate microwaves in the cavity means that we can have a circulating microwave power in the cavity much larger than the power of the input signals.

The first technical requirement of our cavity is that it it support traveling and not standing waves. This consideration is important, because standing waves have nodes and antinodes

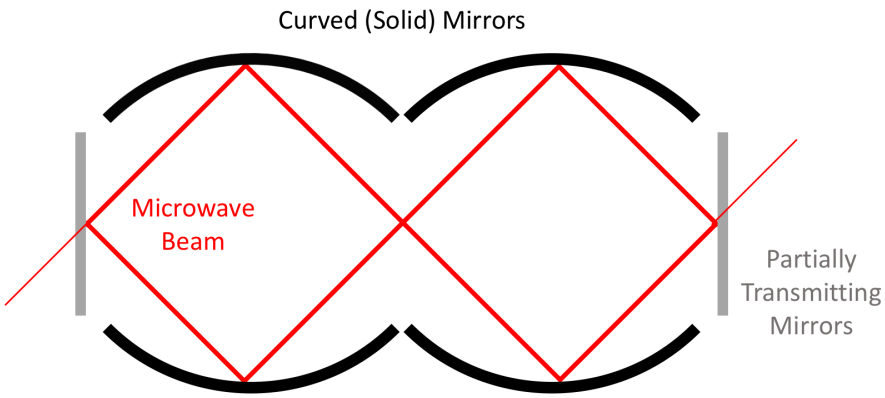

Figure 2: A simple diagram of our cavity, with curved mirrors shown in black, flat (partially transmitting) mirrors shown in grey, and the microwave beam shown in red.

that do not move spatially over time. These nodes and antinodes are spaced out on the order of the wavelength of the wave (for the case of gigahertz-range microwaves, centimeters apart). This is unacceptable, because such a microwave field might interact differently wth different parts of our molecular beam, creating inconsistencies between molecules. The requirement that this be a traveling wave cavity places certain constraints on possible geometric configurations.

Next, we would like our cavity to support multiple frequencies in the gigahertz range at once. We hope to resonate microwaves frequencies of 13.335 GHz, 26.669 GHz, 40.004 GHz, and 53.337 GHz in a single cavity. If we configure the cavity geometry correctly, we ensure that these frequencies are present (in high power) in the cavity, and that other frequencies are not. Specifically, we hope to circulate 1-10 Watts of power in the cavity, while inputting only 10-100 milliwatts.

There are a number of other geometric constraints regarding the phase shifts of waves as they resonate, governed by a the physics of optics and of Gaussian beams. After consideration of these additional constraints, we find that a configuration of four curved mirrors meets our requirements, while also minimizing the number of expensive optical elements. However, without any flat mirrors, it is very hard to adjust the coupling into and out of the cavity. For this reason, we choose to implement a six-mirror setup, with four curved mirrors on the sides, and two (partially-transmitting) flat mirrors on the ends of the cavity. These flat mirrors make it simple and easy to change the cavity coupling when necessary. The curved mirrors are parabolic in the vertical direction (to avoid spherical aberration) and circular in the horizontal direction. A diagram of the cavity configuration is pictured in Figure 2.

We have now assembled our cavity, machined to meet our precise geometric specifications. Waveguides direct electric signals into a microwave horn, which converts the signals into electromagnetic radiation and sends them into the cavity. (A second receiving horn is also used to measure transmission through the cavity.) However, fully assembled, it is difficult to isolate effects of specific cavity parameters. For this reason, I focused on analyzing the

independent behavior of the partially-transmitting mirrors.

4.3 Mirror Transmission

These partially-transmitting mirrors are simply plane mirrors with circular holes in a 2-dimensional array formation. These mirrors play an important role cavity behavior. The fraction of power reflected and transmitted as microwaves enter and exit the cavity determines how microwave power circulates. A theoretical treatment of microwave signals as plane waves incident on an aperture array allows one to predict mirror transmission. This derivation is outlined in the PhD thesis of one of Professor DeMille's former graduate students [5].

The array transmission coefficient, α, is defined to be transmitted power divided by incident power. For sufficiently large arrays, we find that:

$$\alpha_{\text{trans}} = \left(\frac{\pi d^3}{3\lambda s^2}\right)^2$$

where d is the aperture diameter, s is the center-to-center distance between apertures, and λ is the wavelength of the incident radiation. Important to note here is the inverse-square dependence on wavelength, implying that transmission through the mirror, all else held equal, should scale as the square of frequency. This semester, I worked to experimentally verify this predicted relationship.

4.4 Transmission Measurement

To isolate effects of the aperture array transmission, I began by removing the mirrors from the cavity and placing the generating and recieving horns in line, pointing at one another, with a mirror in between the two. The purpose of this geometry was to directly measure the microwave power through the mirror. A microwave generator, the SynthHD (made by Windfreak Technologies), was used to generate electric signals, and a wideband power sensor made by Rohde & Schwarz was used to interpret signals detected by the receiving horn. A diagram of the setup can be seen in Figure 3.

At first, both because the microwave beam tended to diverge and because there were a variety of items in the lab unpredictably reflecting microwaves, it was nearly impossible to discern the signal from background noise. To try and address this issue, I took identical measurements with a the aperture array, a solid (theoretically non-transmitting) mirror of the same size as the aperture array, and nothing in between the generating and receiving horns. I then used these measurements to calculate a transmission coefficient as follows:

$$P_{\text{transmitted}} = \alpha_{\text{trans}} P_{\text{incident}} + P_{\text{background}}$$

We can directly measure transmitted power, and we can take $\alpha = 0$ for the solid, non-transmitting mirror, and $\alpha = 1$ for the case with no mirror in place. Note that incident power is not the same as input power (which we control) becuase the microwaves diverge

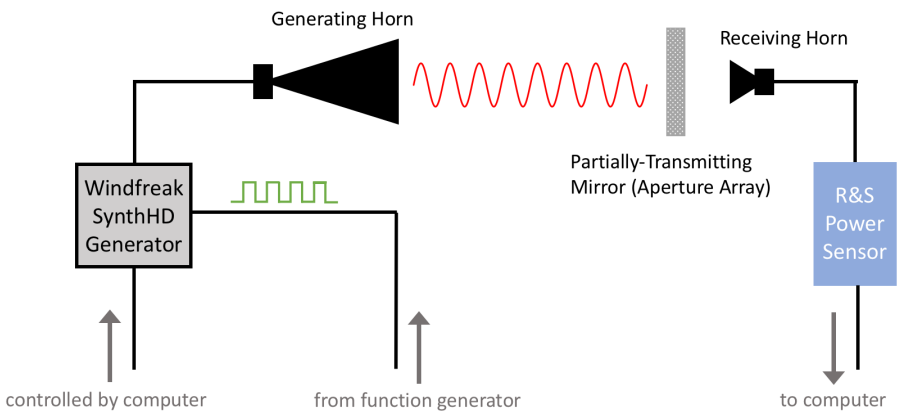

Figure 3: A diagram of the setup used to directly measure aperture array transmission.

and reflect about the lab before they reach the mirror. Still, by taking a measurement with a solid mirror, we can infer the background power, and then by taking a measurement with no mirror, we can calculate the incident power at the location of the mirror. With these two "control" measurements in hand, I could begin to make sense of array transmission measurements. We define P_{array} as the transmitted power with the array in place, P_{solid} with the non-transmitting mirror in place, and P_{open} with no mirror in place. Then naturally,

$$P_{\text{background}} = P_{\text{solid}}$$
$$P_{\text{incident}} = P_{\text{open}} - P_{\text{solid}}$$

and a value for α is calculated according to:

$$\alpha_{\text{trans}} = \frac{P_{\text{array}} - P_{\text{solid}}}{P_{\text{open}} - P_{\text{solid}}}$$

Applying the above methodology provided a framework to calculate trustworthy values for array transmission, however, the transmitted power through the array remained frustratingly small. The values measured with the partially- and non-transmitting mirrors in place were essentially indistinguishable due to random noise in the signal. In hindsight, this should not have been so surprising, given that theory predicts a transmission on the order of 0.1% to 0.5%. Nonetheless, the problem remained that we were unable to discern such small transmission from noise.

The solution to this problem ultimately lay in the use of a triggered input signal, used in a similar way to that in a lock-in amplifier. Using a 1 kHz square wave trigger signal,

we were able to rapidly switch on and off the microwaves coming from the generating horn (also shown in Figure 3). We then took a time sweep over 0.1 seconds (100 periods of the trigger signal) with our power sensor. A fast Fourier transform is then applied to convert the signal from the time domain to the frequency domain. In our analysis, the key assumption we make is that noise radiation is unlikely to *naturally* have a particularly large frequency component at exactly 1 kHz. Therefore, we are able to claim that the power we detect at a frequency of 1 kHz, above the noise level of other frequencies, comes essentially just from our microwave source. To minimize any effects from random noise components that may happen to appear at specific frequencies in a given run, we average the frequency components from 100 different runs in each measurement.

4.5 Results

Using this method of a triggered input signal, we were able to obtain nonzero measurements for aperture array transmission in the following way. We again applied the formula from above, correcting our array measurements with measurements from a solid mirror and with no mirror. Figure 4 illustrates how we are able to discern our signal amidst noise using the fast Fourier transform, for a single run at 11 GHz. Pictured on top is the signal with no mirror, in the middle is the signal with the aperture array, and on the bottom is the signal with the solid mirror. Important to note is that we often see a small peak at 1 kHz with the solid mirror (as in this example), which is most likely due to microwaves from our generator that make their way around the mirror. In a sense, this observation validates our use of the solid mirror so that we can subtract out received microwave power that did not go through the array.

As many (100) trials are averaged, the noise levels lower, and we can see the frequencies at which microwave power is consistently being received. When we subtract off the background signals (also averaged over 100 trials), we are left with data like those shown in Figure 5. To calculate transmitted power, we integrate (technically, sum) over the peak at 1 kHz. From this process, we obtain measurements of α_{trans} for a series of frequencies. Figure 6 shows our final results for array transmission at five frequencies from 10 GHz to 14 GHz. This aperture array had an aperture diameter of 4 mm and a center-to-center spacing of 2.44 mm.

4.6 Discussion

Looking at our data, it is reassuring to see that all of the measured values for transmission lie at least within the ballpark of the predicted values. The frequency dependence we see here is far from quadratic, as the theory predicts. It is not entirely clear why certain frequencies (11 and 12 GHz) behave so unpredictably, but a possible explanation is the creation of standing waves between the mirror and horns. If this were the case, we would expect to see large and unpredictable changes in measurements as the frequency changed. Given this odd behavior, one would assume that systematic errors at least as large as the difference between measured and predicted transmission are affecting our data. Given the presence of these errors, it seems wise to treat even the seemingly accurate measurements (at 10, 13,

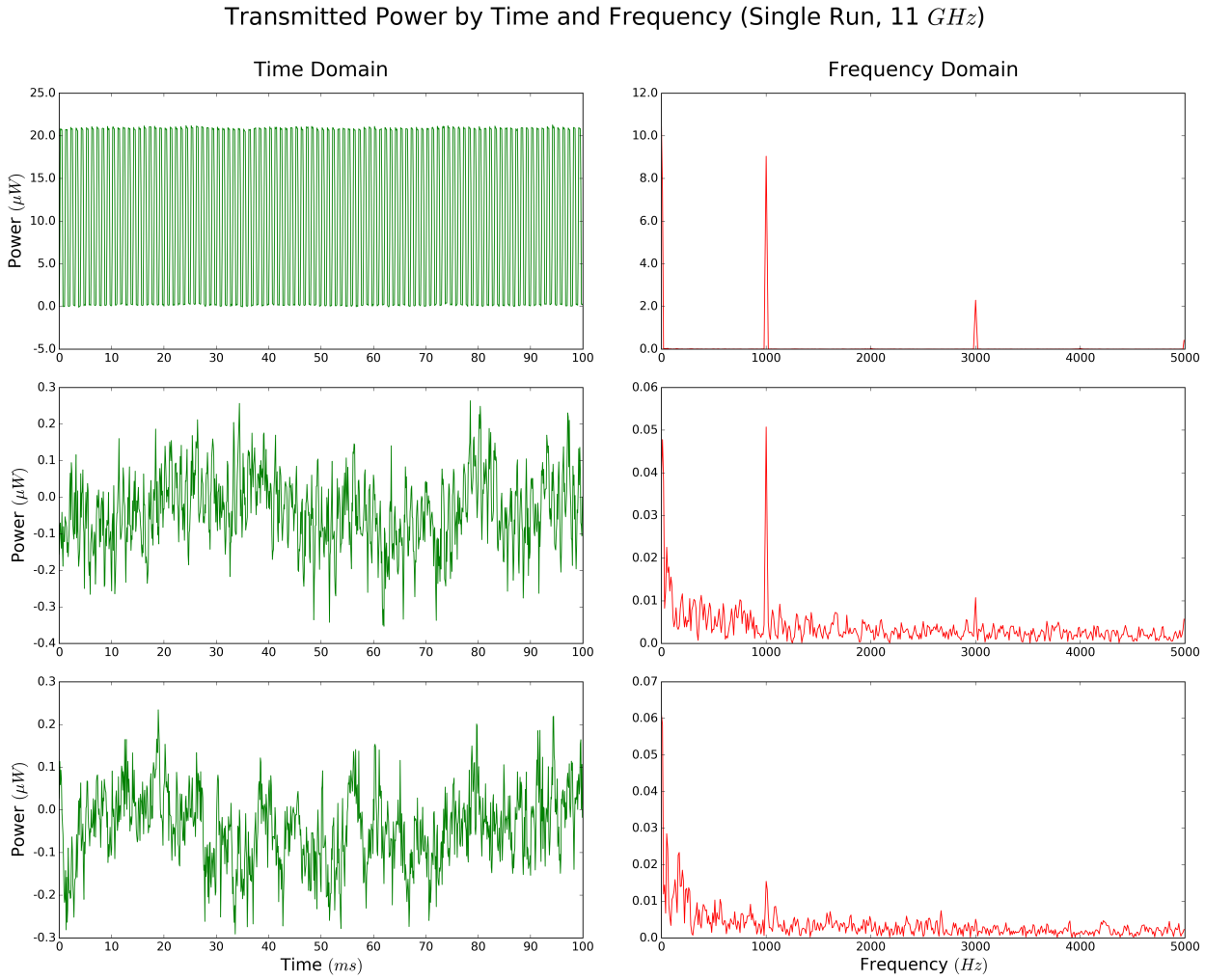

Figure 4: Transmission signals with no mirror (top), the partially-transmitting mirror (middle), and a solid mirror (bottom) represented in both the time and frequency domains.

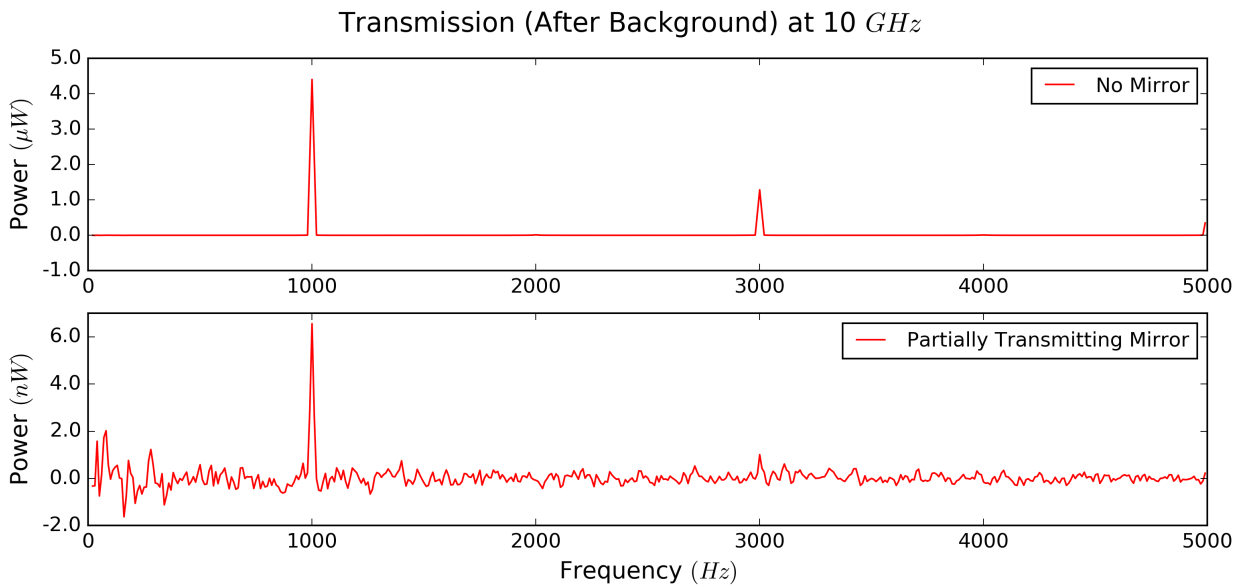

Figure 5: Transmitted power, after subtracting out background power, for 10 GHz. These plots are averages over 100 runs.

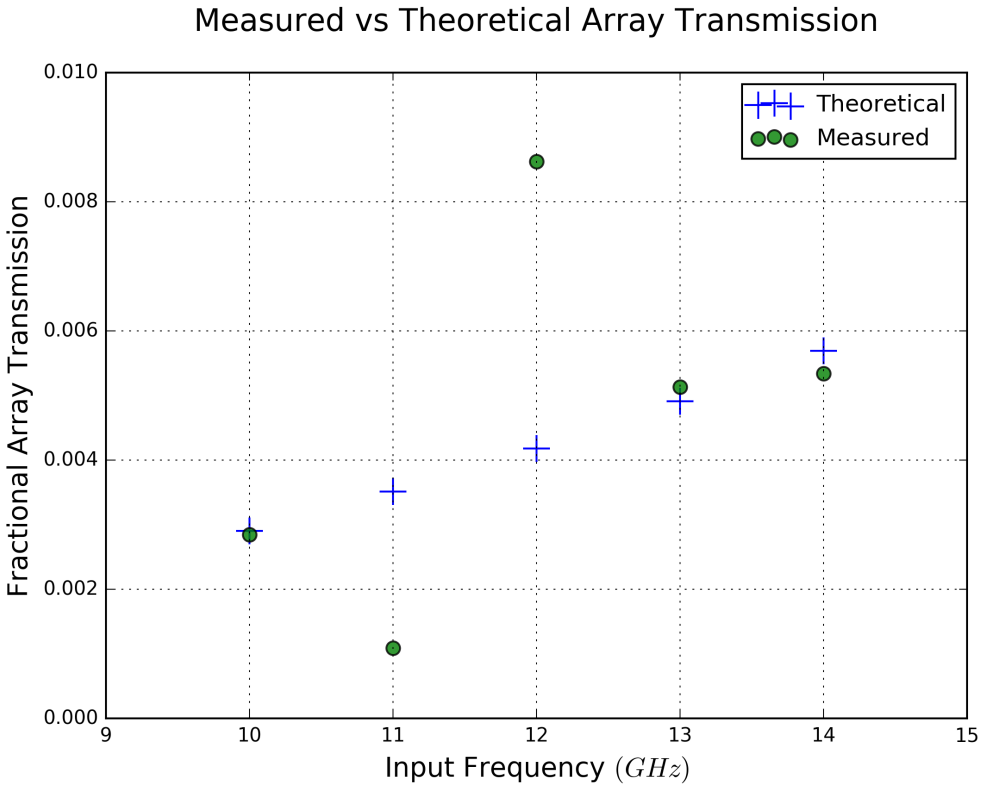

Figure 6: Theoretical and measured values for array transmission at various frequencies.

and 14 GHz) with a fair amount of skepticism. Clearly, there are a number of improvements that could be made to my experimental procedure which would surely yield gains in both precision and accuracy.

4.7 Potential Improvements and Future Work

I was unable to test frequencies lower than 10 GHz because the waveguides we were using attenuated the signal too much, and unable to text frequencies above 14 GHz because of an upper limit of the generating device I was using. A more robust analysis would surely consider other frequencies, and do so taking care to adjust parameters such as the geometry of the setup and the size of the microwave horns. In addition, a better scheme for shielding the setup from background noise would render smaller signals much easier to analyze.

Further study will presumably also need to investigate how changing the aperture spacing and diameter affects measured transmission. My choice to focus on changing frequency was made because it was easy for me to quickly and programatically change frequency. Varying aperture array specifications would have required manually changing mirrors, which seemed likely to introduce systematic errors as pieces were moved and lab conditions changed.

Independent of my actual data, one of my most useful accomplishments was the assembly of an efficient system for measuring array transmission. In order to take measurements, I wrote a series of LabVIEW scripts to control parameters, record information from instruments, and analyze data taken from my setup. These scripts make it straightforward to specify an input microwave frequency and power, trigger the microwave generator, and measure the power received. Then, the raw data is converted from the time domain to the frequency domain (i.e. Figure 4), at which point my program calculates how much power was transmitted at exactly the trigger frequency. My hope is that this software apparatus will allow someone else to, with a more controlled measurement setup, take the more reliable data that will surely be necessary before the final mirror parameters are chosen for the experiment.

5 Acknowledgements

I would like to thank Professor Dave DeMille, for giving me the opportunity to work in his group, and for serving as my advisor for the past year. I would also like to thank all of the members of Professor DeMille's research group who have all individually helped me at one time or another. I need to especially thank Matt Steinecker and Eric Norrgard, who have both spent hours assisting and explaining concepts to me, and have done so with great patience. Lastly, I should thank the SPL machine shop staff, for quickly and expertly addressing all of my machining and building needs.

References

[1] Donghyun Cho, K. Sangster, and E. A. Hinds. Search for time-reversal-symmetry violation in thallium fluoride using a jet source. *Physical Review A*, 44(5):2783, 1991.

[2] W. C. Griffith, M. D. Swallows, T. H. Loftus, M. V. Romalis, B. R. Heckel, and E. N. Fortson. Improved limit on the permanent electric dipole moment of ^{199}Hg. *Phys. Rev. Lett.*, 102:101601, Mar 2009.

[3] M. D. Swallows, T. H. Loftus, W. C. Griffith, B. R. Heckel, E. N. Fortson, and M. V. Romalis. Techniques used to search for a permanent electric dipole moment of the ^{199}Hg atom and the implications for *CP* violation. *Phys. Rev. A*, 87:012102, Jan 2013.

[4] Nicholas R. Hutzler, Maxwell F. Parsons, Yulia V. Gurevich, Paul W. Hess, Elizabeth Petrik, Ben Spaun, Amar C Vutha, David DeMille, Gerald Gabrielse, and John M Doyle. A cryogenic beam of refractory, chemically reactive molecules with expansion cooling. *Physical Chemistry Chemical Physics*, 13(42):18976–18985, 2011.

[5] David Glenn. Development of techniques for cooling and trapping polar diatomic molecules. PhD thesis, Yale University, 2009.